Modeling and Simulation of Bending Moment in Functional Material Coated Silicon Pedestal N/MEMS Resonators

Ritambhara Dash, **A. S. Bhattacharyya***

Department of Metallurgical and Materials Engineering,
Central University of Jharkhand, Ranchi 835222

*arnab.bhattacharya@cuj.ac.in

Abstract
This article presents the modeling and simulation of bending moments in silicon pedestal cantilevers coated with functional materials for N/MEMS resonator applications. Nano- and microelectromechanical systems (N/MEMS) play a pivotal role in modern sensing technologies. Pedestal cantilever sensors leverage functional materials to achieve high sensitivity and selectivity. Coatings such as Ni, Cu-doped ZnO and Zn, Ni-doped CuO enhance performance by tailoring piezoelectric and semiconducting properties. Functional materials such as (Ni, Cu)-doped ZnO, Zn, Ni-doped CuO, Porous Silicon (P-Si), Conducting polymers (CP), bioceramic (HAp), Ti-B-Si-C-N hard nanocomposite and bismaleimide (BMI) polymer coatings were simulated to be applied to the silicon-based pedestal cantilevers using MATLAB. The study examined how these materials influence the bending moment, natural frequency, and displacement under varying loading conditions considering diversified sensing functionalities. A comparative analysis of these materials for sensing different analates under different conditions has been provided.

Keywords: N/MEMS, silicon pedestal cantilevers, functional materials, spring-mass model

1. Introduction

In this age of fast-developing technology, research in novel devices is at the forefront. Functional materials are being developed to be used in the fabrication of these devices. At the same time, the miniaturization of these devices is also being investigated by precision-based methods for their making as well as characterization. The solid-state devices in the current scenario take into consideration the multifaceted properties of materials and find application in every sector of life starting from communication systems, sensors, aerospace, automobile, energy storage, medical diagnostics, etc. The physical properties of the component materials are interlinked making the systems more versatile. The performance in harsh environmental conditions is another matter of concern that is taken care of by making composites or use of protective thin films. This ongoing researches focus on the current scenario of device physics and fabrication techniques based on photonic, magnetic, and electromechanical systems and envisages some state-of-the-art designs in improving their efficiency and longevity [1−3].

1.1 MEMORY DEVICES & DATA STORAGE

Memory devices are mostly based on surface modification of silicon which can be either in the form of thin-film deposition and/or ion beam irradiation. Memristive devices are emerging these days which are used in neuromorphic computing and are based on thin films of Transition metal oxides compatible with CMOS. Going to lower dimensions 0D, 1D, and 2D leads to advances in the nano electronic phenomena, and mimicking a biological neuron becomes more prominent based on Van der Waal's heterojunction-based bio-inspired devices using Artificial Neural Networks (ANN). MoS_2-based mem transistor and CNT are useful neuromorphic systems used in biosensing. The voltage dependence resistance of memristors is sometimes associated with the different phases in the material. Memristors based on Si nano crystallites in SiO_2 matrix by sputtering which is compatible with CMOS and joule heating gets minimized [4-6]

Thin film memristors based on hexagonal boron nitride (hBN) and silicon carbide (SiC) have demonstrated efficient binary resistive memory switching, making them advantageous for advanced memory devices. The integration of silicon-based piezoelectric nano/microelectromechanical systems (N/MEMS) with memristor technology offers enhanced functionality. Nano resistive switch properties in these systems have been investigated using nanoindentation, as reported in amorphous strontium titanate (a-SrTiO3) perovskite memristors [7,8]

Information storage technologies are advancing, with the potential to store single bits in ferromagnetic domains. Researchers have deposited small islands of polycrystalline magnetic thin films and extensively studied their properties for use in magnetic storage devices [8] Key mechanical properties, such as hardness, modulus, fracture toughness, and wear resistance, are critical for optimizing these devices under varying application conditions. Additionally, ion beam irradiation studies have revealed its impact on the morphological properties of thin films, offering new insights into surface engineering. Investigating the correlation between nanomechanical and surface properties is expected to significantly advance the understanding and development of magneto-N/MEMS-based devices.[9]

1.2 SILICON PHOTONIC DEVICES

Silicon-based photonics is being investigated for optical communications and optical interconnects in microelectronic circuits. Many futuristic devices could benefit from the development of basic components such as I/O couplers, modulators, passive functions, and photodetectors. Si is an indirect band gap semiconductor with a band gap of 1.1 eV at room temperature and has limitations in optoelectronic use. However recent technologies in the nano dimension have overcome this problem to some extent. Due to the compatibility with CMOS in fabrication as well as lower cost, silicon photonics has good prospects as next-generation integrated photonics enhances the communication system by many folds. With the introduction of optics inside a high-performance chip, the integration of photonic components and an integrated circuit (IC) on a common chip has resulted in improved IC performance **[10].** The integration of dispersive propagation and nonlinear optics on a Si Microchip has been studied [11]. Increasing communication speed improves cloud service performance [12]. Si photonics must be combined with CMOS in future communication systems. RF transistors were coupled with Si photonics by converting a MOSFET into a MOS capacitor ring modulator [13]. A SiO_2-based blue-violet light-emitting nanocomposite has been developed [14]. Pradhan et al. recently developed an on-chip Raman Laser based on Si nanocavity with a lower threshold power for lasing action due to optical confinement [15]. Ion implantation with Kr+ and As+ causes cubic silicon to become hexagonal and exhibit photoluminescence at 1240 nm, increasing its emissivity [16].

The limitations of lattice mismatch, thermal coefficient, and polarity-induced defects associated with III-V/Si heterojunctions have been addressed as a multi-quantum well laser was epitaxially grown on Si wafers [17]. EDA tools are used to design Si photonics-based devices such as waveguides, splitters, filters, modulators, couplers, and detectors [18]. A silicon nitride-based double micro ring resonator also was recently reported [19]. The laser source is a necessary component of silicon-based photonic integrated circuits (PICs.) Despite the recent demonstration of a germanium laser, practical Si-based light sources remain in short supply. As a result, researchers have concentrated on the heterogeneous integration of III-V semiconductors on silicon [20]. Techniques such as adhesive and molecular wafer bonding are primarily used to densely integrate III-V semiconductors with silicon waveguide circuits. **[21-24].**

The active components in photonic integrated circuits are major heat sources. The thermal resistance between these components and the heat sink i.e good heat dissipation is required for efficient thermal management and will cause a reduction in the operational temperature of the device leading to better performance. The SiO2 cladding layers are the major barriers to heat dissipation. Heat bridges of conducting materials are created to thermally bypass these layers and are called through-thickness thermal vias (TOTV) as shown in Fig 1[25]. Porous Silicon (PS) is an electrochemical derivative of crystalline silicon. Due to its nanostructure, the phenomenon of quantum confinement takes place

in it. This results in its efficient emission of light at room temperature. The microcavities occurring in electrochemically synthesized PS have applications in waveguides **[26-29].**

1.3 ENERGY STORAGE DEVICES

When a client needs power the most, energy from renewable sources can be stored in battery storage, in battery energy storage systems. As the leading storage technology for large-scale plants, lithium-ion batteries, which are utilized in mobile phones and electric vehicles (EVs), allow electrical networks to guarantee a steady supply of renewable energy. Additionally, beyond Li-ion systems and methodologies such as Na-ion, Zn-ion should also be intensively investigated as viable alternative. The battery storage technology will make sure that homes and businesses can be powered by green energy**[30]**

Microelectromechanical systems (MEMS) and nanoelectromechanical systems (NEMS) have emerged as pivotal technologies in the advancement of miniaturized energy storage devices. Their integration into energy storage solutions offers significant benefits, including reduced size, enhanced performance, and compatibility with micro/nanoscale applications. This article explores the role of MEMS and NEMS in energy storage devices, focusing on their design, materials, fabrication techniques, and applications**.[31]**

MEMS-based energy storage devices, such as microbatteries and microsupercapacitors, are engineered to meet the stringent requirements of miniaturized systems. The design process involves creating compact architectures that maximize energy and power densities while ensuring mechanical stability. Techniques like photolithography and etching are employed to fabricate interdigitated electrode patterns on substrates, enabling precise control over device dimensions and performance characteristics. **[32]**

1.4 N/MEMS

N/MEMS (Nano/Micro Electro Mechanical Systems) are miniaturized devices that integrate mechanical and electrical components at micro and nano scales. They are used in sensing, actuation, Signal processing etc. Resonators on the other hand are systems that naturally oscillate with a specific frequency called resonant frequency. They provide electrical, mechanical acoustical optical responses. Tuning fork, cantilever and diaphragms come under the category of resonators. Their design, size and material used affect their performance, Nano- and microelectromechanical systems (N/MEMS) have transformed modern sensing applications. Si-based pedestal cantilevers, with their enhanced sensitivity and reduced noise levels, form the backbone of many N/MEMS sensors. Coating these cantilevers with functional materials such as bismaleimide polymers significantly improves their stability and performance in challenging environments.**[33 -35]**

The increasing demand for compact, sensitive, and selective gas sensors has spurred significant research in microelectromechanical systems (MEMS). Pedestal cantilever sensors have garnered attention due to their high sensitivity and versatility. Integrating porous silicon (Psi) as a structural material enhances gas sensing performance owing to its large specific surface area and tuneable optical and electrical properties.The properties of nanomaterials and small-scale fabrication techniques have envisioned novel devices applicable in daily life as well as specific areas. Nano/electro-mechanical systems (N/MEMS) require materials to sustain any operating conditions and be more efficient at the same time. New designs in improving the efficiency of these devices are being thought of in the form of nanomechanical resonators and the usage of magnetic as well as optical materials. The interconnects and the fiber-optic systems are being upgraded for faster communications as well as longevity. A huge application of these devices is in the biomedical field where biocompatibility is a major issue. **[36]**

1.5 NANOMECHANICAL RESONATORS

Nanomechanical resonator-based sensing devices are used in medical diagnostics based on their high frequency dynamic behavior. Cantilevers fall into the category of Nanomechanical resonators. It also resembles a resonator whose shape is like that of a nanowire clamped at one end. As the

surface to volume ratio of a nanowire resonator increases due to scaling down, the surface stress plays a crucial role in the mechanical behavior of a resonator. Piezoresistive MEMS cantilever are used for vapor phase analysis of volatile compounds and gas. Studies were done to address the mass sensitivity issues and fracture associated with bioceramic and nanocomposite coatings-based cantilever resonators. The studies how the sensing performance can be determined or tuned. A cantilever structure fabricated through solid -state lithography and micromachining at nanometer dimension which vibrate at a fixed tuneable frequency are called nanomechanical resonators and have many technological applications especially as sensors. The frequency of vibration is dependent on the mass getting attached with the free end as inversely proportional to $\sqrt{m}$. Linear resonators clamped at one fixed end can be modified by changing the length. There are called resonators as they can couple with each other. The separating distance between them is also a deciding factor. Fig 1 shows a schematic representation of the abovementioned facts. Four resonators marked as R B N and G **[37 – 40]**

1.6 Cantilever

Cantilever beams are critical components in N/MEMS devices, serving as resonators and sensors for physical, chemical, and biological analytes The performance of N/MEMS resonators relies heavily on the choice of materials. Recent advances in materials have focused on improving sensitivity, stability, frequency tunability, and reducing energy dissipation. The coating of functional materials on silicon pedestal cantilevers is a smart addition interms of enhancing and diversification of the sensing abilities of the fabricated device structure. Bending moments, a key factor in cantilever design, are affected by material properties such as Young’s modulus, density, and coating thickness. This study models these effects and simulates them using MATLAB. Cantilever beams are critical components in N/MEMS devices, serving as resonators and sensors for physical, chemical, and biological parameters. The coating of functional materials on silicon pedestal cantilevers improves their mechanical and sensing properties. The performance of MEMS and NEMS resonators relies heavily on the choice of materials. Recent advances in materials have focused on improving sensitivity, stability, frequency tunability, and reducing energy dissipation. Below are the major material advancements:**[41,42]**

1.7 Material advancement in N/MEMS resonators

Silicon-Based Materials like Single-Crystal Silicon (SCS) are widely used due to excellent mechanical properties and low internal damping. They are suitable for high-frequency applications and large-scale production. Silicon Carbide (SiC) on the other hand posse’s high thermal conductivity and resistance to chemical and mechanical wear. They are Ideal for harsh environment applications like aerospace and automotive industries. Porous Silicon have the advantage of lightweight, possessing tuneable porosity, and high surface area which enhances their sensitivity for gas and bio-sensing applications.Porous silicon (PSi) is an emerging material in the field of gas sensing due to its high surface area, tunable porosity, and excellent compatibility with microfabrication techniques. This article focuses on the development of pedestal cantilever sensors fabricated from porous silicon for gas sensing applications. The article covers the fabrication process, material characterization, sensing performance, and a detailed mathematical modeling of cantilever dynamics. Comparative analyses of PSi-based and bulk silicon cantilever sensors are presented to emphasize the advantages of PSi in gas detection. The large surface area of P-Si enables the adsorption of more gas molecules, enhancing sensitivity. The functionalization of P-Si with chemical groups (e.g., amines or thiols) also improves selectivity for specific gases. PSi cantilever sensors can detect trace levels of gases such as NOx and CO_2 for air quality monitoring.Detection of hazardous gases like methane or ammonia ensures workplace safety. PSi-based sensors functionalized with biomolecules enable detection of volatile organic compounds (VOCs) in breath analysis for disease diagnosis. Porous silicon-based pedestal cantilever sensors shall offer enhanced sensitivity and selectivity for gas sensing applications. The high surface area and tunable porosity make PSi an ideal material for detecting trace gases. While challenges like thermal stability and fabrication complexity remain, ongoing research promises to unlock the full potential of PSi in advanced sensing technologies.**[43-52]** A comparison of P-Si with bulk silicon is given in **Table 3**

Table **3:** Comparative analysis of bulk Si and P-Si based cantilevers performances

Property	Bulk Si Cantilever	Porous Si Cantilever
Density	2.33 g/cm³	~1.5 g/cm³ (depending on porosity)
Surface Area	Low	High
Gas Sensitivity	Moderate	High
Thermal Stability	High	Moderate
Fabrication Complexity	Low	Moderate

Nanocomposite hard coats integrate ceramic and polymer phases, providing high hardness, wear resistance, and thermal stability. ZnO's piezoelectric properties are enhanced by doping with Ni and Cu. Ni increases the conductivity, while Cu modifies the defect density, improving sensitivity and response time.CuO, a p-type semiconductor, benefits from Zn and Ni doping, which increases its surface area, conductivity, and catalytic activity for gas sensing applications**[53, 54].**

Zinc Oxide (ZnO) has high piezoelectric coefficient and ease of deposition on substrates. It is used in energy harvesting and vibration-based sensors. Aluminum Nitride (AlN) offers better thermal stability than ZnO and Is suitable for RF MEMS filters and high-frequency oscillators. Lead Zirconate Titanate (PZT) has high piezoelectric performance, ideal for actuation and sensing. It is however Limited by environmental concerns due to lead content**.[55, 56]**

2D Materials like Graphene has exceptional mechanical strength, electrical conductivity, and flexibility and finds usage in ultra-sensitive mass and pressure sensors. Molybdenum Disulfide (MoS_2) having high Young's modulus and piezoelectric properties can be applied to flexible and stretchable resonators**.[57,58]**

Nanocomposite Materials like Metal-Oxide Composites (eg. Ni-doped ZnO, CuO-Zn composites. have enhance piezoelectric and sensing properties. Polymer-Based Nanocomposites are lightweight and cost-effective materials for bio-MEMS applications. Bismaleimide polymers are high-performance materials known for their superior thermal stability, chemical resistance, and mechanical durability. This article investigates their application as coatings for silicon-based pedestal cantilever sensors. The mechanical, thermal, and sensing properties of these sensors are studied in detail, with an emphasis on environmental monitoring and biochemical sensing. Mathematical modeling of cantilever dynamics is presented, alongside a comparative analysis of uncoated and coated cantilevers. They are chosen for their: high thermal stability: Up to 350°C.m Chemical resistance (Ideal for corrosive environments) and mechanical properties: for durability under stress. They are thermosetting resins derived from maleimide monomers. Their molecular structure features strong covalent bonds, imparting high thermal and chemical stability.The Thermal Stability imparts resistance to high-temperature fluctuations ensuring consistent sensor performance. Apart from being chemically inert (which provides protection against corrosive gases and liquids, they are lightweight and Flexible hence do not add significant mass, preserving the sensor's resonance frequency**.[59- 63]**

High-Q Dielectrics and Metals Diamond and Diamond-Like Carbon (DLC): have extremely high stiffness and thermal conductivity and are used for high-Q resonators operating at GHz frequencies. Gold and Platinum Thin Films: are also commonly used for their excellent conductivity in RF

MEMS resonators, which however have the limitations of increased damping due to high density. Vanadium Dioxide (VO_2): shows metal-to-insulator transition properties. enables tuneable resonators and reconfigurable RF systems. Ge-Sb-Te Alloys are used in thermal sensors and energy-efficient MEMS devices. Bio-Compatible Materials like Polydimethylsiloxane (PDMS): make Flexible and bio-compatible, used for bio-MEMS devices. Titanium-Based Alloys: are ideal for medical implants due to their bio-compatibility and corrosion resistance. Shape Memory Alloys (SMAs) like Nickel-Titanium based NITINOL are used for actuators in MEMS. exhibits reversible deformation under temperature changes. Magneto strictive Materials: like Terfenol-D, Fe-Ga alloys. provide magnetic-field-driven actuation for resonators. Multilayer Coatings: like SiO_2/Si_3N_4 layers have the advantages for thermal isolation and mechanical enhancement. Heterostructures with 2D Materials: Combination of graphene with traditional semiconductors for improved performance. Integration with existing fabrication processes. Trade-offs between sensitivity, stability, and cost. Long-term reliability in harsh environments and development of environmentally friendly materials (e.g., lead-free piezoelectric) are some of the challenges in Material advancements The enhanced integration of 2D materials into standard MEMS/NEMS fabrication. and quantum materials for ultra-sensitive applications. continue to drive innovation in N/MEMS resonators, expanding their application domains and improving their overall performance. This article explores the synthesis, deposition, and performance analysis of bismaleimide polymer coatings on Si-based pedestal cantilever sensors. **[64-73].** A comparison of the basic properties significant of cantilever-based sensing of different functional materials is given in **Table 1**. The objective of this article is to compare the mechanical, thermal, and sensing characteristics of different materials and assess their suitability for specific applications.

Table 1: A comparison of the physical parameters significant for sensing applications

Material	Young's Modulus (GPa)	Thermal Stability (°C)	Sensing Type	Key Features
Nanocomposite Hard Coats	200-300	700	Mechanical/ Environmental	High wear resistance, robust mechanical properties
Bismaleimide Polymers	2-4	350	Environmental	Lightweight, thermally stable
Ni, Cu-Doped ZnO	120-140	400	Mechanical/ Piezoelectric	Enhanced piezoelectric sensitivity
Zn, Ni-Doped CuO	70-90	300	Gas/ Biochemical	High surface area, catalytic efficiency

2. **Materials and Methods**

Fabrication process includes Nanocomposites coatings developed by physical vapor deposition (PVD) like magnetron sputtering on silicon substrates. Doped ZnO and CuO: RF magnetron

sputtering or sol-gel techniques. A uniform layer of bismaleimide polymer is applied on the Si substrate by spin-coating at 3000 RPM. The coating is cured at 200°C for 2 hours to ensure cross-linking of polymer chains. The cantilever structure is fabricated using photolithography and etching.

Bending moments, a key factor in cantilever design, are affected by material properties such as Young's modulus, density, and coating thickness. This study models these effects and simulates them using MATLAB.

The bending moment (**M**) at a distance along the cantilever is given by:
M(x) = -F (L - x); where F: Applied force at the free end of the cantilever., L: Length of the cantilever.and x: Distance from the fixed end. The deflection ***y(x)*** of the cantilever is derived using the bending moment and flexural rigidity (**E I**):

$y(x) = F/6EI\ (Lx^3 - x^4)$, where E: Young's modulus of the material.I: Moment of inertia of the cross-section, .b: Width of the cantilever.and t: Thickness of the cantilever. The natural frequency (***f_o***) is influenced by the coating material: $f_0 = \frac{1}{2\pi}\sqrt{\frac{k}{m_{eff}}}$. where k: Spring constant. m_{eff}: Effective mass of the cantilever. **Table 2** below shows the parameters considered for simulation The geometric parameters included a cantilever length (L): 200 µm and width (b): 50 µm. The MATLAB codes for comparative parameter estimation is given in **Appendix A**

Table 2 Modulus, density and coating thickness initialized for simulation

Material	Young's Modulus (E)	Density (ρ)	Coating Thickness (t)
Silicon (substrate)	169 GPa	2330 kg/m³	2 µm
Ni, Cu-doped ZnO	100 GPa	5600 kg/m³	1 µm
Zn, Ni-doped CuO	70 GPa	6300 kg/m³	1 µm
Bismaleimide Polymer	5 GPa	1200 kg/m³	2 µm

The cantilever beam can be modelled as a simple spring-mass-damper system. The governing equation for the system is:$m\ddot{x} + c\dot{x} + kx = F(t)$, where m is the effective mass of the cantilever. C is the damping coefficient; k is the spring constant (related to stiffness) and x is the displacement of the cantilever and F(t) is the external force acting on the cantilever. The natural frequency (ω_o) of the system is given by:$\omega_0 = \sqrt{\frac{k}{m}}$, $f_0 = \frac{1}{2\pi}\sqrt{\frac{k}{m}}$ and the damping ratio (ζ) and quality factor expressed as $\zeta = \frac{c}{2\sqrt{km}}$ and $Q = \frac{1}{2\zeta}$ respectively.

In the resonator dynamics Deflection Resonant frequency Damping factor are the main parameters which are again affected by materials selection and design of the system. The deflection Δz, occurring in a cantilever due to an applied force F is governed by the mechanical and geometrical parameters like elastic modulus (E), beam thickness(t), width(b), length(L) and spring constant

(stiffness) as $\Delta z=(4FL^3)/(Ebt^3)=F/K$. A slight alteration is found when the design changes from clamped-free structure to clamped - clamped structure(**Fig 3**).The deflections can be associated with non linear impact parameters $\delta = (g/L)^2$ ·For Cantilever structure used in sensing, having a clamped-free structure, change in δ and due to which, a variation in sensitivity takes place (Fig) ❙ Solution to this problem has been proposed in the form of pedestal design.

The MATLAB Code for Spring-Mass Model Simulation is given in **Appendix B**. The fundamental resonance frequency changes when the cantilever beam gets coated as

$$f_0 = \frac{1.875^2}{2\pi L^2}\sqrt{\frac{Et}{12\rho(1+k_m)}}$$

where E is the modulus of the material, t the total thickness including the coating thickness and km the added mass ratio due to the coating. The deflection (Δz) of the coated cantilever under applied force F is then given as $\Delta Z = \frac{4FL^3}{Ebt^3}$ and the sensitivity (S) being the ratio of deflection to applied force is $S = \frac{\Delta Z}{F} = \frac{4L^3}{Ebt^3}$. The parmeters used for the simulation was modulus (E) and density (ρ) as given in **Table 3** . The geometrical dimensions of the cantilevers however remained unchanged

Table 3: Elastic modulus and density of different functional materials used in Spring-mass model-based simulation

Material	Modulus (GPa)	Density (kg/m^3)
Silicon	169	2330
(Ni, Cu) doped ZnO	100	5600
(Zn, Ni) doped CuO	70	6300
Bismaleimide	5	1200

In case of porous silicon (P-Si), the effective mass gets affected by porosity (ϕ) as $m_{eff} = \rho_{bulk}(1 - \phi)V$, and the frequency shift due to gas absorption is $\Delta f = -\frac{f_o}{2}\frac{\Delta m}{m_{eff}}$.

3. Results and Discussion

The simulation shows that the bending moment and deflection are significantly influenced by the material properties of the coating. A comparative analysis of the maximum bending moment, max deflection natural (resonant) frequency and damping coefficient obtained for the different materials is given in **Table 4 (a, b)** The results obtained from the spring mass model-based simulations are given in **Table 5**

Table 4: (a, b) Comparative analysis of maximum bending moment, maximum deflection and natural frequency, and damping coefficient for the different materials used

Material	Max Bending Moment (ÂµN · m)	Max Deflection (nm)	Natural Frequency (kHz)
Silicon (uncoated)	0.04	0.45	195.5
Ni, Cu-doped ZnO	0.06	0.60	123.2
Zn, Ni-doped CuO	0.07	0.70	115.8
Bismaleimide Polymer	0.03	1.20	192.1

Material	Young's Modulus (E)	Density (ρ)	Damping Coefficient (c)
Silicon (substrate)	169 GPa	2330 kg/m³	0.001 Ns/m
Ni, Cu-doped ZnO	100 GPa	5600 kg/m³	0.002 Ns/m
Zn, Ni-doped CuO	70 GPa	6300 kg/m³	0.003 Ns/m
Bismaleimide Polymer	5 GPa	1200 kg/m³	0.005 Ns/m

Material	Resonance Frequency (kHz)	Deflection (nm)	Sensitivity (nm/N)
Silicon (uncoated)	195.5	0.45	0.003
Ni, Cu-doped ZnO	123.2	0.60	0.004
Zn, Ni-doped CuO	115.8	0.70	0.005
Bismaleimide Polymer	192.1	1.2	0.010

The comparative analysis depicting deflection and natural frequency was asper codes given in **APPENDIX C**. The corresponding plots are given in **Fig 3(d).**The uncoated structure consisting of bare silicon had the highest frequency and lowest deflection. The lowest frequency was shown by Ni,Zn doped CuO. As stiffness (K) is inversely proportional to deflection and the natural frequency is proportional to$\sqrt{}$ K, a higher deflection infers lower vibrational frequency. The relation can be expressed as $f_o = n / \sqrt{(F\ \delta)} = n / \sqrt{S}$ where n is a constant $n = 1/2\pi\sqrt{m}$. and $S = \delta/F$ is the sensitivity The mass (m) is therefore a parameter which quantifies intensely the deflection and frequency are coupled or how sensitive is the structure. A lower mass will cause higher coupling and therefore more sensitive. The BMI polymers showed the highest deflection as being a polymeric having the lowest mass amongst all others.

4. Conclusion

The MATLAB simulation confirms that functional material coatings alter the bending moment, deflection, and natural frequency of silicon pedestal cantilevers. The findings highlight the importance of material selection for optimizing the performance of N/MEMS resonators in sensing applications. This study demonstrates the potential of MATLAB for modeling and simulation of functional material-coated silicon pedestal cantilever sensors. The simulation results highlight the impact of material properties on resonance frequency, deflection, and sensitivity. MATLAB-based analysis provides valuable insights into optimizing cantilever designs for specific sensing applications. was observed that, the coatings of high-density materials (e.g., Zn, Ni-doped CuO) reduces the resonance frequency however, lightweight coatings like that of bismaleimide polymer maintain higher resonance frequencies. The functional materials with lower Young's modulus, such as bismaleimide polymers, on the other hand, exhibit higher deflection and sensitivity.

BIBLIOGRAPHY

1. Recent Advances in All-Solid-State Batteries for Commercialization. Mater. Chem. Front. 2024, 8 (1), 23–41. https://doi.org/10.1039/D3QM01171B.

2. Solid-State Single-Photon Sources: Recent Advances for Novel Quantum Materials in Photonics. Adv. Funct. Mater. 2023, 33 (12), 2315936. https://doi.org/10.1002/adfm.202315936.

3. Wang, Z.; Wang, Y.; Wang, W.; Yu, M.; Xiong, C.; Renner, H.; Baehr-Jones, T.; Hochberg, M.; Pantazis, Y. Integrated Silicon Photonic MEMS. Microsyst. Nanoeng. 2023, 9, 30. https://doi.org/10.1038/s41378-023-00498-z.
4. Zhang, F.; Yang, Y.; Choi, S.; Rehman, S.; Ali, F.; Li, L.; Jiang, J.; Lee, J.; Lee, H.; Choi, W. MoS_2 Memtransistors Fabricated by Localized Helium Ion Beam Irradiation for Neuromorphic Computing. ACS Nano 2019, 13 (11), 13016–13024. https://doi.org/10.1021/acsnano.9b07421.
5. Zidan, M. A.; Strachan, J. P.; Lu, W. D. The Future of Electronics Based on Memristive Systems. Nature Electronics 2018, 1, 22–29. https://doi.org/10.1038/s41928-017-0006-8.
6. Yang, J. J.; Strukov, D. B.; Stewart, D. R. Memristive Devices for Computing. Nature Nanotechnology 2013, 8, 13–24. https://doi.org/10.1038/nnano.2012.240.
7. F.Qin et al Materials Advances, Volume 5, Issue 10, 20 May 2024, Pages 4209-4220 https://doi.org/10.1039/d3ma01142a
8. J. Bisquert et al APL Mach. Learn. 1, 036101 (2023) https://doi.org/10.1063/5.0153289
9. Aich, P.; Meneghini, C.; Tortora, L. Advances in Structural and Morphological Characterization of Thin Magnetic Films: A Review. Materials 2023, 16, 7331. https://doi.org/10.3390/ma16237331
10. Shahbaz, M.; Butt, M.A.; Piramidowicz, R. Breakthrough in Silicon Photonics Technology in Telecommunications, Biosensing, and Gas Sensing. Micromachines 2023, 14, 1637. https://doi.org/10.3390/mi14081637
11. Sirleto, L.; Righini, G.C. An Introduction to Nonlinear Integrated Photonics Devices: Nonlinear Effects and Materials. Micromachines 2023, 14, 604. https://doi.org/10.3390/mi14030604
12. Ogawa, K. Increase in Modulation Speed of Silicon Photonics Modulator with Quantum-Well Slab Wings: New Insights from a Numerical Study. Photonics 2024, 11, 535. https://doi.org/10.3390/photonics11060535
13. Radamson HH, Zhu H, Wu Z, He X, Lin H, Liu J, Xiang J, Kong Z, Xiong W, Li J, et al. State of the Art and Future Perspectives in Advanced CMOS Technology. Nanomaterials. 2020; 10(8):1555. https://doi.org/10.3390/nano10081555
14. Romanov, I., Parkhomenko, I., Vlasukova, L., Wendler, E., & Komarov, F. (2024). Intense violet electroluminescence of thin SiO2 layers with SnO2 nanocrystals. Results in Optics, 17(100750), 100750. https://doi.org/10.1016/j.rio.2024.100750
15. Pradhan, A. K., Sen, M., & Datta, T. (2022). LED pumped Raman laser: Towards the design of an on-chip all-silicon laser. Optics and Laser Technology, 147(107634), 107634. https://doi.org/10.1016/j.optlastec.2021.107634
16. Nikolskaya, A. A., Korolev, D. S., Mikhaylov, A. N., Konakov, A. A., Belov, A. I., Marychev, M. O., Murtazin, R. I., Pavlov, D. A., & Tetelbaum, D. I. (2020). Photoluminescence of silicon at 1235 nm produced by irradiation of SiO2/Si with Kr+ ions and subsequent high-temperature annealing. Surface & Coatings Technology, 386(125496), 125496. https://doi.org/10.1016/j.surfcoat.2020.125496
17. Li, Q., & Lau, K. M. (2017). Epitaxial growth of highly mismatched III-V materials on (001) silicon for electronics and optoelectronics. Progress in Crystal Growth and Characterization of Materials, 63(4), 105–120. https://doi.org/10.1016/j.pcrysgrow.2017.10.001
18. C. Sun, L. Du and J. Zhao, “A brief review of design and simulation methodology in silicon photonics,” in Tsinghua Science and Technology, vol. 27, no. 3, pp. 526-533, June 2022, doi: 10.26599/TST.2021.9010038.
19. Butt, M.A.; Kozłowski, Ł.; Golas, M.; Slowikowski, M.; Filipiak, M.; Juchniewicz, M.; Bieniek-Kaczorek, A.; Dudek, M.; Piramidowicz, R. Numerical and Experimental Demonstration of a Silicon Nitride-Based Ring Resonator Structure for Refractive Index Sensing. Appl. Sci. 2024, 14, 6082. https://doi.org/10.3390/app14146082
20. Shekhar, S., Bogaerts, W., Chrostowski, L. et al. Roadmapping the next generation of silicon photonics. Nat Commun 15, 751 (2024). https://doi.org/10.1038/s41467-024-44750-0

21. Park, J.-S.; Tang, M.; Chen, S.; Liu, H. Heteroepitaxial Growth of III-V Semiconductors on Silicon. Crystals 2020, 10, 1163. https://doi.org/10.3390/cryst10121163
22. Liu J, Sun X, Camacho-Aguilera R, Kimerling LC, Michel J.Ge-on-Si laser operating at Room temperature. Opt Lett 2010; 35:679–81.
23. Dong P, Hu T-C, Zhang L, Dinu M, Kopf R, Tate A, Buhl L, Neilson DT, Luo X, Liow T-Y, Lo G-Q, Chen Y-K. 1.9 μm hybrid silicon/III-V semiconductor laser. IEE Electronic Letts 2013; 49:664–6.
24. A. Novack et al.: Progress in silicon platforms for integrated optics, Nanophotonics 2014; 3(4-5): 205–214
25. Pedro Andrei Krochin Yepez, Ulrike Scholz, Jan Niklas Caspers, and Andre Zimmermann, IEEE Photonics Journal, Vol. 11, No. 4, August 2019 6602415
26. L. Canham. Handbook of porous silicon (pp. 163-170). Berlin, Germany: Springer International Publishing (2014).
27. L. Pavesi, Porous silicon dielectric multilayers and microcavities. Riv. Nuovo Cim. 20, 1 (1997).
28. L Pavesi and P Dubos Random porous silicon multilayers: application to distributed Bragg reflectors and interferential Fabry – Pérot filters Semicond. Sci. Technol. 12 570 (1997)
29. H. Saha, S.Dey, C.Pramanik, J.Das, T.Islam Porous Silicon Based Sensors Amenable to Smart Sensing, anuary 2006, In book: Encyclopedia of sensors, Chapter: Encyclopedia of Sensors Craig A Grimes, Elizabeth C Dickey, Michael V. Pishko (Eds)American Scientific Publishers (ASP)
30. Nikolskaya, A. A., Korolev, D. S., Mikhaylov, A. N., Konakov, A. A., Belov, A. I., Marychev, M. O., Murtazin, R. I., Pavlov, D. A., & Tetelbaum, D. I. (2020). Photoluminescence of silicon at 1235 nm produced by irradiation of SiO_2/Si with Kr^+ ions and subsequent high-temperature annealing. Surface & Coatings Technology, 386(125496), 125496. https://doi.org/10.1016/j.surfcoat.2020.125496
31. Jolayemi, B.; Buvat, G.; Roussel, P.; Lethien, C. Emerging Capacitive Materials for On-Chip Electronics Energy Storage Technologies. Batteries 2024, 10, 317. https://doi.org/10.3390/batteries10090317
32. Ma, Y., Wang, S. & Wu, ZS. Photolithographic Microfabrication of Microbatteries for On-Chip Energy Storage. Nano-Micro Lett. 17, 105 (2025). https://doi.org/10.1007/s40820-024-01625-9
33. Craighead, H. G. Nanoelectromechanical Systems. Science 2000, 290 (5496), 1532–1535. https://doi.org/10.1126/science.290.5496.1532.
34. Ekinci, K. L.; Roukes, M. L. Nanoelectromechanical Systems. Rev. Sci. Instrum. 2005, 76 (6), 061101. https://doi.org/10.1063/1.1927327.
35. Bhushan, B. Nanotribology and Nanomechanics of MEMS/NEMS and BioMEMS/BioNEMS Materials and Devices. Microelectron. Eng. 2007, 84 (3), 387–412. https://doi.org/10.1016/j.mee.2006.10.115.
36. Nikolic, M.V.; Milovanovic, V.; Vasiljevic, Z.Z.; Stamenkovic, Z. Semiconductor Gas Sensors: Materials, Technology, Design, and Application. Sensors 2020, 20, 6694. https://doi.org/10.3390/s20226694
37. R. Dash, A.S. Bhattacharyya, Materials Today: Proceedings, 66 7 (2022) 3233-3237
38. R. Dash, R. P. Kumar, K. Bhattacharyya, A. S. Bhattacharyya, IOP- Engineering Research Express, 4 (2022) 045012
39. M.G. Azandariani, M. Gholami, A. Nikzad, Adv. Nano Res., 12 (2022) 37-47.
40. M.N. Balchi, M. N. (2022) Adv. Nano Res 13 (2022),147-164.
41. Ilic, B.; Czaplewski, D.; Craighead, H. G.; Neuzil, P.; Campagnolo, C.; Batt, C. A. Single Cell Detection with Micromechanical Oscillators. J. Vac. Sci. Technol. B 2001, 19 (6), 2825–2828. https://doi.org/10.1116/1.1417520.
42. Verbridge, S. S.; Shapiro, D. F.; Craighead, H. G.; Parpia, J. M. Macroscopic Tuning of Nanoresonators: Effects of Cavity Geometry and Surface Stress. Nano Lett. 2007, 7 (6), 1728–1735. https://doi.org/10.1021/nl0703578.

43. Canham, L. T. Silicon Quantum Wire Array Fabrication by Electrochemical and Chemical Dissolution of Wafers. Appl. Phys. Lett. 1990, 57 (10), 1046–1048. https://doi.org/10.1063/1.103561.
44. Gole, J. L.; Sailor, M. J.; Brumlik, C. J.; Nasr, K. A.; Searson, P. C. Porous Silicon in Sensor Applications: An Overview. Adv. Mater. 1999, 11 (6), 456–459. https://doi.org/10.1002/(SICI)1521-4095(199905)11:6<456::AID-ADMA456>3.0.CO;2-Y.
45. Bisi, O.; Ossicini, S.; Pavesi, L. Porous Silicon: A Quantum Sponge Structure for Silicon Based Optoelectronics. Surf. Sci. Rep. 2000, 38 (1–3), 1–126. https://doi.org/10.1016/S0167-5729(99)00012-6.
46. Aroutiounian, V. M.; Shahnazaryan, G. E.; Soukiassian, L. E. Porous Silicon Sensors. J. Phys. D: Appl. Phys. 2001, 34 (18), 2650–2671. https://doi.org/10.1088/0022-3727/34/18/201.
47. Sailor, M. J. Porous Silicon in Practice: Preparation, Characterization and Applications. Wiley-VCH 2012, ISBN 978-3-527-40798-8.
48. Cui, Y.; Lieber, C. M. Functional Nanoscale Electronic Devices Assembled Using Silicon Nanowire Building Blocks. Science 2001, 291 (5505), 851–853. https://doi.org/10.1126/science.291.5505.851.
49. Baratto, C.; Faglia, G.; Comini, E.; Sberveglieri, G.; Pan, Z.; Wang, Z. L. Functionalized Porous Silicon for Gas Sensing Applications. Appl. Phys. Lett. 2003, 82 (10), 1613–1615. https://doi.org/10.1063/1.1558981.
50. Sailor, M. J.; Link, J. R. Applications of Porous Silicon in Biosensors, Separation, and Surface Chemistry. Chem. Commun. 2005, 11, 1373–1382. https://doi.org/10.1039/B416968F.
51. Roy, S.; Basu, S. Improved Gas Sensing Properties of Semiconductor Functionalized Porous Silicon. Sens. Actuators B Chem. 2002, 92 (1–2), 90–96. https://doi.org/10.1016/S0925-4005(03)00203-5.
52. Star, A.; Gabriel, J. P.; Bradley, K.; Gruner, G. Gas Sensing with Combined Functionality of Porous Silicon and Carbon Nanotubes. Nano Lett. 2003, 3 (4), 459–463. https://doi.org/10.1021/nl034040v.
53. Kumar, M.; Bhushan, B.; Gupta, M. Nanocomposite Hard Coatings for Wear Resistance and Thermal Stability. Surf. Coat. Technol. 2010, 205 (5), 1256–1264. https://doi.org/10.1016/j.surfcoat.2010.08.063.
54. Li, Y.; Mo, R.; Liu, J.; Wang, X. Enhanced Gas Sensing Properties of Ni and Cu-Doped ZnO Nanostructures. Sens. Actuators B Chem. 2013, 176, 560–568. https://doi.org/10.1016/j.snb.2012.09.035.
55. Wang, Z. L.; Song, J. Piezoelectric Nanogenerators Based on Zinc Oxide Nanowire Arrays. Science 2006, 312 (5771), 242–246. https://doi.org/10.1126/science.1124005.
56. Dubois, M. A.; Muralt, P. Properties of Aluminum Nitride Thin Films for Piezoelectric Transducers and Microwave Filter Applications. Appl. Phys. Lett. 1999, 74 (20), 3032–3034. https://doi.org/10.1063/1.123872.
57. 1. Novoselov, K. S.; Geim, A. K.; Morozov, S. V.; Jiang, D.; Zhang, Y.; Dubonos, S. V.; Grigorieva, I. V.; Firsov, A. A. Electric Field Effect in Atomically Thin Carbon Films. Science 2004, 306 (5696), 666–669. https://doi.org/10.1126/science.1102896.
58. 2. Bertolazzi, S.; Brivio, J.; Kis, A. Stretching and Breaking of Ultrathin MoS_2. ACS Nano 2011, 5 (12), 9703–9709. https://doi.org/10.1021/nn203879f.
59. Ramgir, N.; Datta, N.; Kaur, M.; Kailasaganapathi, S.; Aslam, M.; Debnath, A. K.; Sharma, R. K.; Singh, V.; Muthe, K. P. Metal-Oxide Nanostructures for Gas Sensing: A Review. Appl. Phys. Rev. 2016, 3 (3), 031301. https://doi.org/10.1063/1.4959913.
60. Mai, V. T.; Yoo, H.; Son, S. J.; Oh, H. J.; Kim, Y. S. Highly Sensitive Flexible Pressure Sensors Based on Ni-Doped ZnO Nanoparticles. ACS Appl. Mater. Interfaces 2020, 12 (23), 26129–26139. https://doi.org/10.1021/acsami.0c05479.
61. Ma, P.; Siddiqui, N. A.; Marom, G.; Kim, J.-K. Dispersion and Functionalization of Carbon Nanotubes for Polymer-Based Nanocomposites: A Review. Compos. Part A Appl. Sci. Manuf. 2010, 41 (10), 1345–1367. https://doi.org/10.1016/j.compositesa.2010.07.003.

62. Mittal, V.; Matsko, N. B. Biodegradable Polymer Nanocomposites: A State-of-the-Art Review. J. Mater. Sci. 2012, 47 (20), 7431–7447. https://doi.org/10.1007/s10853-012-6517-6.
63. Gholampour, A.; Ozbakkaloglu, T. A Review of Natural Fiber Composites: Properties, Modification and Processing Techniques, Characterization, Applications. J. Mater. Sci. 2020, 55 (3), 829–892. https://doi.org/10.1007/s10853-019-03990-y.
64. O'Connell, C.; McNally, T.; Pötschke, P.; Krause, B.; Halley, P.; Murphy, M.; Carrillo, J.; Bielawski, C. W.; Brétigny, C.; Broz, M. E. Characterization of Multiphase Polymer Systems with Carbon Nanotubes. Carbon 2008, 46 (5), 1203–1224. https://doi.org/10.1016/j.carbon.2008.02.011.
65. Yang, K.; Guo, X.; Tang, Q.; Guo, Q.; Liu, Z. Diamond-Like Carbon Coatings for MEMS Resonators: High-Q Applications. ACS Appl. Mater. Interfaces 2016, 8 (12), 8185–8193. https://doi.org/10.1021/acsami.6b01347.
66. Lee, K.; Kim, H. Gold and Platinum Thin Films for MEMS and RF Devices. Thin Solid Films 2009, 517 (17), 4921–4925. https://doi.org/10.1016/j.tsf.2009.02.109.
67. Cao, J.; Fan, W.; Wu, H.; Zheng, H.; Gong, J. Vanadium Dioxide Nanostructures with Metal-to-Insulator Transition Properties for MEMS Applications. Nano Lett. 2010, 10 (7), 2667–2673. https://doi.org/10.1021/nl101231d.
68. Kolobov, A. V.; Tominaga, J. Chalcogenides as Photonic and Thermal Sensors: Ge–Sb–Te Alloys. Appl. Phys. Lett. 2004, 85 (5), 780–782. https://doi.org/10.1063/1.1778703.
69. Shin, D.; Park, S. J.; Kim, S.; Lee, M. H. Polydimethylsiloxane (PDMS) in Bio-MEMS Devices: Synthesis and Applications. Biomaterials 2013, 34 (25), 6137–6144. https://doi.org/10.1016/j.biomaterials.2013.04.058.
70. Park, J. B.; Lakes, R. S. Titanium Alloys for Medical Implants. J. Biomed. Mater. Res. 1992, 26 (12), 1557–1576. https://doi.org/10.1002/jbm.820261205.
71. Morgan, N. B. Shape Memory Alloys: Nickel-Titanium (NITINOL) Actuators in MEMS Applications. Mater. Sci. Eng. A 2004, 378 (1–2), 16–23. https://doi.org/10.1016/j.msea.2003.10.326.
72. Ried, R.; Kremer, F.; Büttner, H. Magnetostrictive Terfenol-D and Fe-Ga Alloys for MEMS Resonators. J. Appl. Phys. 2003, 93 (10), 7286–7291. https://doi.org/10.1063/1.1559330.
73. Lee, H. J.; Lee, J. H.; Choi, J.; Lee, K. Heterostructures of Graphene with Traditional Semiconductors for MEMS/NEMS Applications. Nano Res. 2017, 10 (9), 3167–3180. https://doi.org/10.1007/s12274-017-1594-1.
74. R. Dash, D. Sharma, A. S. Bhattacharyya, Thermal Management and optical entrapment in multilayered porous silicon for use as waveguide Techrxiv 2022.

SUPPLEMENTARY/APPENDIX

A. MATLAB codes for estimating the bending moment and deflection in cantilever beams

```
% Bending Moment and Deflection in Cantilever Beams

% Parameters
L = 200e-6; % Length (m)
b = 50e-6; % Width (m)
t = [2e-6, 1e-6, 1e-6, 2e-6]; % Thickness (m) for different materials
E = [169e9, 100e9, 70e9, 5e9]; % Young's Modulus (Pa)
rho = [2330, 5600, 6300, 1200]; % Density (kg/m^3)
materials = {'Silicon', 'Ni, Cu-doped ZnO', 'Zn, Ni-doped CuO', 'Bismaleimide
Polymer'};
F = 1e-6; % Applied force (N)

% Loop through each material
for i = 1:length(materials)
    % Moment of inertia
    I = b * t(i)^3 / 12;
    % Flexural rigidity
    EI = E(i) * I;
    % Distance along the cantilever
    x = linspace(0, L, 100);
    % Bending moment
    M = -F * (L - x);
    % Deflection
    y = (F / (6 * EI)) * (L * x.^3 - x.^4);

    % Plot results
    figure;
    subplot(2, 1, 1);
    plot(x * 1e6, M * 1e6);
    xlabel('Position along cantilever (µm)');
    ylabel('Bending Moment (µN·m)');
    title(['Bending Moment for ', materials{i}]);

    subplot(2, 1, 2);
    plot(x * 1e6, y * 1e9);
    xlabel('Position along cantilever (µm)');
    ylabel('Deflection (nm)');
    title(['Deflection for ', materials{i}]);
end
```

B. MATLAB codes for spring-mass model of cantilevers

```
% Spring-Mass Model for Cantilever Sensor

% Parameters
L = 200e-6; % Length (m)
b = 50e-6; % Width (m)
t = 2e-6; % Thickness (m)
materials = {'Silicon', 'Ni, Cu-doped ZnO', 'Zn, Ni-doped CuO', 'Bismaleimide
Polymer'};
E = [169e9, 100e9, 70e9, 5e9]; % Young's Modulus (Pa)
rho = [2330, 5600, 6300, 1200]; % Density (kg/m^3)
c = [0.001, 0.002, 0.003, 0.005]; % Damping Coefficient (Ns/m)

% Calculations
```

```
for i = 1:length(materials)
    % Effective mass
    m = rho(i) * L * b * t;
    % Spring constant
    k = E(i) * b * t^3 / (4 * L^3);
    % Resonance frequency
    f0 = (1 / (2 * pi)) * sqrt(k / m);
    % Damping ratio
    zeta = c(i) / (2 * sqrt(k * m));
    % Quality factor
    Q = 1 / (2 * zeta);

    % Display results
    fprintf('Material: %s\n', materials{i});
    fprintf('Resonance Frequency: %.2f kHz\n', f0 / 1e3);
    fprintf('Damping Ratio: %.4f\n', zeta);
    fprintf('Quality Factor: %.2f\n\n', Q);
end
```

C. Comparative analysis of natural frequency and deflections for different functional materials

```
octave:1> % Parameter Estimation and Comparative Plotting for Functional Materials

% Parameters
L = 200e-6; % Length of cantilever (m)
b = 50e-6; % Width (m)
t = [2e-6, 1e-6, 1e-6, 2e-6]; % Thickness (m) for different materials
E = [169e9, 100e9, 70e9, 5e9]; % Young's Modulus (Pa)
rho = [2330, 5600, 6300, 1200]; % Density (kg/m^3)
materials = {'Silicon', 'Ni, Cu-doped ZnO', 'Zn, Ni-doped CuO', 'Bismaleimide
Polymer'};
F = 1e-6; % Applied force (N)

% Preallocation
freq = zeros(1, length(materials));
maxDeflection = zeros(1, length(materials));

% Loop through materials
for i = 1:length(materials)
    % Moment of inertia
    I = b * t(i)^3 / 12;
    % Effective mass
    m_eff = rho(i) * L * b * t(i);
    % Spring constant
    k = (3 * E(i) * I) / (L^3);
    % Natural frequency
    freq(i) = (1 / (2 * pi)) * sqrt(k / m_eff);
    % Max deflection
    maxDeflection(i) = (F * L^3) / (3 * E(i) * I);
end

% Plotting Results
figure;
subplot(2, 1, 1);
bar(freq);
set(gca, 'XTickLabel', materials);
ylabel('Frequency (Hz)');
title('Natural Frequency Comparison');

subplot(2, 1, 2);
bar(maxDeflection * 1e9);
set(gca, 'XTickLabel', materials);
ylabel('Deflection (nm)');
title('Maximum Deflection Comparison');
```

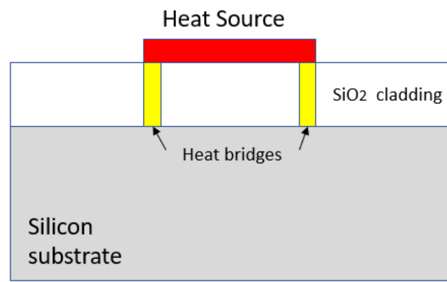

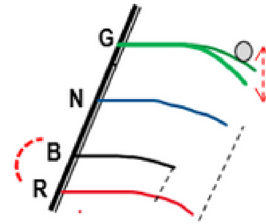

Fig 1. Heat bridges as TOTV for heat dissipation **[25]. (b)** Cantilever based nanomechanical resonator for sensing**[40]**

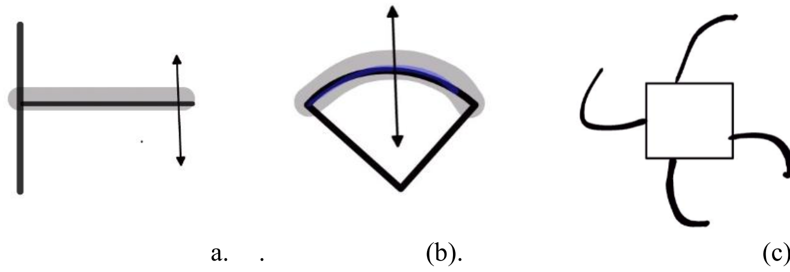

a. . (b). (c)

Fig 2 . (a)Cantilever (single clamp -free) (b) double clamped beam and (c) pedestal design

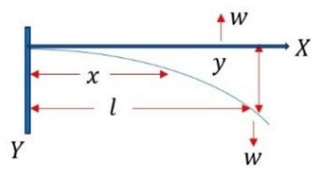

$$\delta = \frac{wl^3}{Ybd^3}$$

$$w\ (= mg)$$

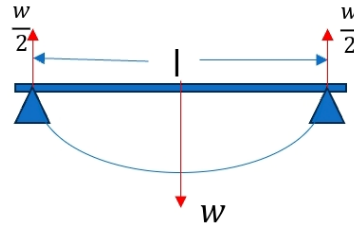

$$\delta = \frac{wl^3}{48YAK^2}$$

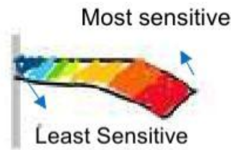

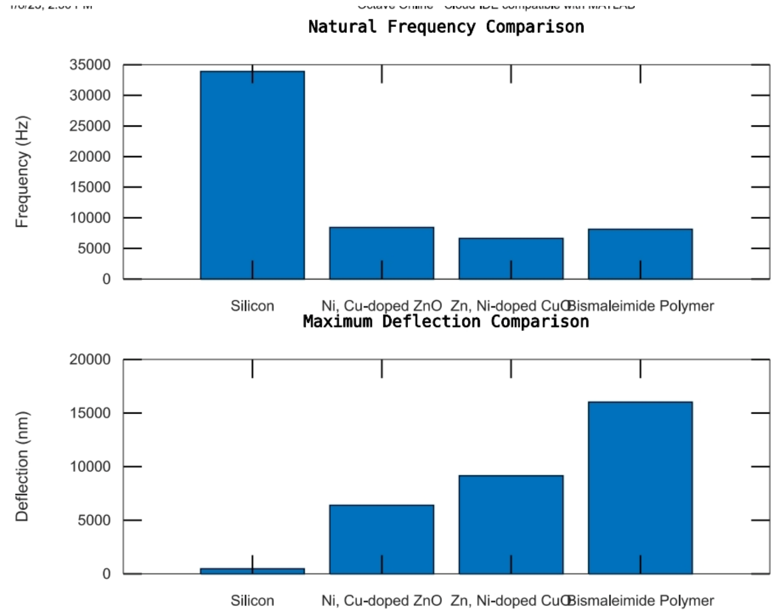

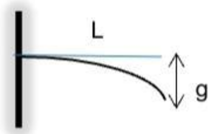

$$\delta = \left(\frac{g}{L}\right)^2$$

non-linear impact factor

Fig 3 Deflections due to force(weight) applied in (a)clamped free Cantilever beams and (b) Clamped-clamped beams (c) sensitivity changes associated with cantilever structure and (d) variations in natural frequency and deflection for use of different functional materials in the beam